Lattice Boltzmann simulations of contact line motion. I. Liquid-gas systems

A. J. Briant,[1] A. J. Wagner,[2] and J. M. Yeomans[1]
[1]*Department of Physics, Theoretical Physics, University of Oxford, 1 Keble Road, Oxford OX1 3NP, United Kingdom*
[2]*Department of Physics, North Dakota State University, Fargo, North Dakota 58105, USA*
(Received 26 July 2003; published 22 March 2004)

We investigate the applicability of a mesoscale modeling approach, lattice Boltzmann simulations, to the problem of contact line motion in one and two component, two phase fluids. In this, the first of two papers, we consider liquid-gas systems. Careful implementation of the thermodynamic boundary condition allows us to fix the static contact angle in the simulations. We then consider the behavior of a sheared interface. We show that the contact line singularity is overcome by evaporation or condensation near the contact line which is driven by the curvature of the diffuse interface. An analytic approximation is derived for the angular position of a sheared interface.

DOI: 10.1103/PhysRevE.69.031602 PACS number(s): 68.03.−g, 68.08.−p, 47.55.Kf

I. INTRODUCTION

When a droplet comes into contact with a solid surface capillary forces drive it towards equilibrium. The equilibrium state may be a droplet with a finite contact angle (known as partial wetting) or a thin film covering the surface (known as complete wetting) [1]. The process of the droplet reaching equilibrium is known as spreading and corresponds to the three phase line, or contact line between gas, liquid, and solid, moving over the surface. Wetting and spreading phenomena are important to many industrial processes where a thin coating of a given substance is required for a specific use (e.g., a lubricant, a paint, or ink) or where wetting properties may inhibit or enhance a desired fluid flow (e.g., extracting oil from porous media, the design of microfluidic devices).

The equilibrium properties of partial wetting have been understood for many years. The contact angle can be calculated from a balance of forces at the contact line. The surface tensions between pairs of phases balance to determine the contact angle θ_w via Young's law

$$\cos\theta_w = \frac{\sigma_{sg} - \sigma_{sl}}{\sigma}, \tag{1}$$

where σ, σ_{sg}, and σ_{sl} are the liquid-gas, solid-gas, and solid-liquid surface tensions [2].

The nonequilibrium situation of a droplet moving over a surface (or a solid object being withdrawn from a liquid) is not so well understood. A fluid mechanical treatment of a contact line moving relative to a solid surface, under the usual no slip boundary conditions for the fluid velocity, shows that an infinite drag force is exerted upon the solid; the solid is thus dragged with the fluid and no movement of the contact line, relative to the solid, is permitted [3–5].

Since the posing of this problem there have been many ways suggested to overcome the classical paradox. One approach is to relax the no-slip condition at the surface within a distance *s*, the slip length, of the contact line. The Navier-Stokes equations are solved by means of a matched asymptotic expansion in two small parameters [6–9]. For a droplet of viscosity η, macroscopic radius *R*, surface tension σ, moving relative to a surface with velocity *U*, the two small parameters are $Ca(=\eta U/\sigma)$, called the capillary number, and $\epsilon(=s/R)$. The inertial terms of the Navier-Stokes equations are neglected (the slow flow approximation) and the resulting Stokes equations are solved within either two or three regions. The outer solution, valid at distances far from the contact line, is matched to the inner solution, which is valid at distances of order *s* from the contact line. The matching procedure may also require an additional region, known as the intermediate region. The interface shapes and flow fields predicted have been confirmed by experiments at length scales of order 10^{-6} m [10–15]. However, while these solutions give the interface shapes and flow fields on macroscopic scales, the slip introduced is phenomenological and the physics in the immediate vicinity of the contact line is no clearer. Furthermore, the macroscopic predictions of different slip models are the same [5], meaning that no macroscopic measurement can be used to infer microscopic properties.

Molecular dynamics simulations have been used to probe the immediate vicinity of the contact line [16–18] and to evaluate the no-slip boundary condition [19–21]. These studies suggest that some slip of fluid molecules takes place in a variety of situations. Recent work by Denniston and Robbins [20] examines the flow near solid walls of a miscible binary fluid with concentration gradients driving diffusion. They report a breakdown in one slip model which is often used, in which the difference between the fluid and solid velocities is proportional to the viscous shear stress at the contact point. The results of these molecular dynamics simulations offer a possible explanation of contact line motion, namely, that the no-slip condition breaks down at very small distance from the contact line.

Alternative explanations of contact line motion exist which do not rely on the breakdown of the no slip condition. Effective slip of the interface relative to the wall may be generated by mechanisms missing from sharp interface treatments and recently diffuse interface models have been applied to the contact line problem [22–24]. Examining a one component system, Seppecher found that curvature of the interface near the contact line leads to mass transport across

the interface [22]. In a binary fluid system, Jacqmin [23] and Chen *et al.* [24] demonstrated that diffusive transport of fluid can lead to effective slip of the interface at the contact line.

With the advent of mesoscopic simulation methods, it seems timely that a mesoscale modeling method be applied to the problem of contact line motion to gain new perspectives on solutions offered in the literature. The first steps of applying lattice Boltzmann to this problem have already appeared [25–27]. Grubert and Yeomans [25] used a binary lattice Boltzmann approach to measure contact angles of small droplets. More recently Desplat *et al.* [26] and Briant *et al.* [27] described how wetting boundary conditions may be implemented in the lattice Boltzmann method.

The aim of this and the following paper is to apply the lattice Boltzmann approach to modeling partial wetting and contact line motion in one and two component, two phase fluids. Thus we elucidate the mechanisms available for contact line motion in diffuse interface treatments subject to strict no slip boundary conditions on the fluid velocity. In this paper, we examine the contact line motion in a one-component system, showing how interfacial curvature drives evaporation or condensation near the contact line. In a companion paper we consider binary systems, where a dynamic length scale emerges which controls diffusion near the contact line. In contradiction to the work of Chen *et al.* [24] we find that diffusive effects do not increase as the contact line speed is reduced.

This paper breaks down as follows. In Sec. II we briefly present the lattice Boltzmann scheme used. In Sec. III we describe the boundary conditions needed to model wetting properties within the lattice Boltzmann framework and the shear boundary conditions used for the velocity field. Section IV presents simulation results for sheared liquid-gas systems which show that the velocity perpendicular to the liquid-gas interface is proportional to its radius of curvature. Section V presents a simple scaling argument for the constant of proportionality. In Sec. VI we derive a partial differential equation for the angular position of a sheared interface and hence discuss the emergence of a dynamic contact angle. We close in Sec. VII with a discussion of the results.

II. THE LATTICE BOLTZMANN MODEL

In this section we review the free energy approach for the lattice Boltzmann method, first introduced by Swift *et al.* in 1995 [28]. We describe the basic scheme in Sec. II A by showing the lattice Boltzmann equation used, detailing the collision term and equilibrium distribution, presenting the Navier-Stokes level equations and finally introducing the collision and streaming steps needed for numerical computation. In Sec. II B we show how the free energy for the liquid-gas system can model two bulk phases at different densities and interfaces of finite width between the phases. We detail the precise form of the free energy used and calculate the surface tension of the interfaces.

A. Free energy lattice Boltzmann

The lattice Boltzmann method simulates the time evolution of density functions $f_{\sigma i}(\mathbf{x},t)$ which represent the mass density at position $\mathbf{x}$ and time t moving with velocity $\mathbf{e}_{\sigma i}$. Both time and space are discretized such that in a time Δt the mass with velocity $\mathbf{e}_{\sigma i}$ advects to a neighboring lattice site $\mathbf{x}+\mathbf{e}_{\sigma i}\Delta t$. In this paper we use a two-dimensional square lattice with N_x and N_y lattice sites in the x and y directions. The lattice sites are labeled by coordinates (i,j) with $i=1,2,3,\ldots,N_x$ and $j=1,2,3,\ldots,N_y$. The lattice spacing is Δx and we use a square lattice with nine velocity vectors (the so-called D2Q9 lattice). The velocity vectors are labeled by the subscript $\sigma=\mathbf{e}_{\sigma i}^2/c^2$, where $c=\Delta x/\Delta t$, the lattice speed. For $\sigma=1$ and 2 the label i runs from 1 to 4 (this label i is distinct from the coordinate i as clear from the context). The zero speed vector is labeled $\mathbf{e}_{0,0}$. Physical quantities are related to moments of $f_{\sigma i}$. The fluid density n and velocity $\mathbf{u}$ are defined at each site by

$$\sum_{\sigma,i} f_{\sigma i}=n, \tag{2}$$

$$\sum_{\sigma,i} f_{\sigma i}e_{\sigma i\alpha}=nu_\alpha, \tag{3}$$

where $e_{\sigma i\alpha}$ is the α component of the vector $\mathbf{e}_{\sigma i}$ and α is either of the lattice directions, x or y.

The distributions $f_{\sigma i}$ are evolved according to a lattice Boltzmann equation assuming a single relaxation time approximation

$$f_{\sigma i}(\mathbf{x}+\mathbf{e}_{\sigma i}\Delta t,t+\Delta t)-f_{\sigma i}(\mathbf{x},t)=-\frac{1}{\tau_f}(f_{\sigma i}-f_{\sigma i}^{eq}), \tag{4}$$

where τ_f is the nondimensional relaxation time and $f_{\sigma i}^{eq}$ is an equilibrium distribution function. The right-hand side of Eq. (4) is the Bhatnagar-Gross-Krook collision operator [29] which was first proposed for use in lattice Boltzmann models by Qian *et al.* [30]. This form of the collision operator represents a simplification over early models and dictates that $f_{\sigma i}$ relaxes towards the local equilibrium distribution $f_{\sigma i}^{eq}$ with a single characteristic time τ_f. The equilibrium distribution determines the physics inherent in the simulation. A power series in the local velocity is assumed [31]

$$f_{\sigma i}^{eq}=A_\sigma+B_\sigma e_{\sigma i\alpha}u_\alpha+C_\sigma u^2+D_\sigma e_{\sigma i\alpha}e_{\sigma i\beta}u_\alpha u_\beta + G_{\sigma\alpha\beta}e_{\sigma i\alpha}e_{\sigma i\beta}, \tag{5}$$

where summation over repeated Cartesian indices is understood.

The coefficients A_σ, B_σ, C_σ, D_σ, and $G_{\sigma\alpha\beta}$ are determined by placing constraints on the moments of $f_{\sigma i}^{eq}$. In order that the collision term in Eq. (4) conserves mass and momentum the first two moments of $f_{\sigma i}^{eq}$ are constrained by

$$\sum_{\sigma,i} f_{\sigma i}^{eq}=n, \tag{6}$$

$$\sum_{\sigma,i} f_{\sigma i}^{eq}e_{\sigma i\alpha}=nu_\alpha. \tag{7}$$

The next moment of $f_{\sigma i}^{eq}$ is chosen such that the continuum macroscopic equations approximated by the evolution scheme (4) correctly describe the hydrodynamics of a one component, nonideal fluid. This gives

$$\sum_{\sigma,i} f_{\sigma i}^{eq} e_{\sigma i\alpha} e_{\sigma i\beta} = P_{\alpha\beta} + n u_\alpha u_\beta + \nu_{\text{visc}} [u_\alpha \partial_\beta (n) + u_\beta \partial_\alpha (n) + u_\gamma \partial_\gamma (n) \delta_{\alpha\beta}], \tag{8}$$

where $\nu_{\text{visc}} = c^2(\tau_f - 1/2)\Delta t/3$ is the kinematic shear viscosity and $P_{\alpha\beta}$ is the pressure tensor. The first formulation of the model omitted the third term in Eq. (8) and was not Galilean invariant. Holdych *et al.* [32] showed that the addition of this term led to any non-Galilean invariant terms being of the same order as finite lattice corrections to the Navier-Stokes equations. In order to fully constrain the coefficients A_σ, B_σ, C_σ, D_σ, and $G_{\sigma\alpha\beta}$ a fourth condition is needed [33], which is

$$\sum_{\sigma i} f_{\sigma i}^{eq} e_{\sigma i\alpha} e_{\sigma i\beta} e_{\sigma i\gamma} = \frac{nc^2}{3} (u_\alpha \delta_{\beta\gamma} + u_\beta \delta_{\alpha\gamma} + u_\gamma \delta_{\alpha\beta}). \tag{9}$$

The values of the coefficients can be determined by a well established procedure [33]. For completeness we give the coefficients in Appendix A.

The analysis of Holdych *et al.* in Ref. [32] shows that the evolution scheme (4) approximates the continuity equation

$$\partial_t n + \partial_\alpha (n u_\alpha) = 0 \tag{10}$$

and the following Navier-Stokes level equation:

$$\begin{aligned}\partial_t (n u_\alpha) + \partial_\beta (n u_\alpha u_\beta) = & -\partial_\beta P_{\alpha\beta} + \nu_{\text{visc}} \partial_\beta [n\{\partial_\beta u_\alpha + \partial_\alpha u_\beta + \delta_{\alpha\beta} \partial_\gamma u_\gamma\}] - \frac{3\nu_{\text{visc}}}{c^2} \partial_\beta [u_\alpha \partial_\gamma P_{\beta\gamma} + u_\beta \partial_\gamma P_{\alpha\gamma} + \partial_\gamma (n u_\alpha u_\beta u_\gamma)] \\ & - \frac{3\nu_{\text{visc}}}{c^2} \partial_\beta [(\partial_n P_{\alpha\beta}) \partial_\gamma (n u_\gamma)] - \frac{3\nu_{\text{visc}}^2}{c^2} \partial_\beta [u_\alpha \partial_\gamma (u_\beta \partial_\gamma n + u_\gamma \partial_\beta n + \delta_{\gamma\beta} u_\lambda \partial_\lambda n)] \\ & - \frac{3\nu_{\text{visc}}^2}{c^2} \partial_\beta [u_\beta \partial_\gamma (u_\alpha \partial_\gamma n + u_\gamma \partial_\alpha n + \delta_{\alpha\gamma} u_\lambda \partial_\lambda n)] + \frac{3\nu_{\text{visc}}^2}{c^2} \partial_\beta [\partial_t (u_\alpha \partial_\beta n + u_\beta \partial_\alpha n + \delta_{\alpha\beta} u_\lambda \partial_\lambda n)].\end{aligned} \tag{11}$$

The top line is the compressible Navier-Stokes equation while the subsequent lines are error terms, which are of order Mach number squared.

For the purposes of computation the evolution Eq. (4) is split into two distinct steps, which can be thought of as a collision step and a streaming step. To facilitate this we introduce (purely for numeric convenience) a new field at each lattice site $f_{\sigma i}^*(\mathbf{x},t)$, so that the collision step is defined by

$$f_{\sigma i}^*(\mathbf{x},t) = f_{\sigma i}(\mathbf{x},t) + \frac{1}{\tau_f}(f_{\sigma i}^{eq} - f_{\sigma i}) \tag{12}$$

and the streaming step by

$$f_{\sigma i}(\mathbf{x}, t+\Delta t) = f_{\sigma i}^*(\mathbf{x} - \mathbf{e}_{\sigma i}\Delta t, t). \tag{13}$$

One lattice Boltzmann step is considered to be one collision step and one streaming step at each site.

We have, then, described a framework for a one component free energy lattice Boltzmann. The properties of the fluid are determined by the choice of pressure tensor $P_{\alpha\beta}$ which we now go on to describe.

B. Thermodynamics of the fluid

The equilibrium properties of a system with no surfaces can be described by a Landau free energy functional

$$\Psi_b = \int dV \left[\psi(T,n) + \frac{\kappa}{2} (\partial_\alpha n)^2 \right] \tag{14}$$

subject to the constraint

$$M = \int dV n, \tag{15}$$

where $\psi(T,n)$ is the free energy density of bulk phases, κ is a constant related to the surface tension, M is the total mass of fluid, and the integrations are over all space. The second term in Eq. (14) gives the free energy contribution from density gradients in an inhomogeneous system.

The free energy density can be conveniently expressed in terms of an excess free energy density $W(n,T)$ via

$$\psi(T,n) = W(n,T) + \mu_b n - p_b, \tag{16}$$

where $\mu_b (= \partial_n \psi|_{n=n_b})$ is the bulk chemical potential and p_b is the bulk pressure. We choose W to be the simplest excess free energy function

$$W(\nu,\tau) = p_c (\nu^2 - \beta\tau)^2, \tag{17}$$

where $\nu = (n - n_c)/n_c$ and $\tau = (T_c - T)/T_c$ are a reduced density and temperature. T_c, p_c, and n_c are the critical temperature, pressure, and density, respectively, and β is a constant.

This simple choice of excess free energy (rather than the traditional van der Waals free energy, for example) enables us to calculate the wall-fluid surface tensions in closed form later (see Sec. III A). For reference the free energy density of the model is

$$\psi = p_c(\nu+1)^2(\nu^2-2\nu+3-2\beta\tau), \tag{18}$$

the bulk chemical potential is

$$\mu_b = \frac{4p_c}{n_c}(1-\beta\tau) \tag{19}$$

and the bulk pressure is

$$p_b = p_c(1-\beta\tau)^2. \tag{20}$$

For $T<T_c$ there are two bulk phases, with densities n_l and n_g equal to $n_c(1+\sqrt{\beta\tau})$ and $n_c(1-\sqrt{\beta\tau})$, respectively.

In addition to uniform phases $n=n_g$ or n_l, the free energy also allows an interface of the form $n=n_c\{1+\sqrt{\beta\tau}\tanh[x/(\sqrt{2}\xi)]\}$ between two phases with width ξ and surface tension σ. It can be shown that

$$\xi = \sqrt{\frac{\kappa n_c^2}{4\beta\tau p_c}}, \tag{21}$$

$$\sigma = \tfrac{4}{3}\sqrt{2\kappa p_c}(\beta\tau)^{3/2}n_c. \tag{22}$$

Thus the equilibrium properties of the model are determined by the choice of free energy.

The free energy enters the lattice Boltzmann algorithm via the pressure tensor $P_{\alpha\beta}$. Since the free energy function and total mass constraint are independent of position, it follows from Noether's theorem that in equilibrium conservation of momentum takes the form

$$\partial_\beta P_{\alpha\beta} = 0 \tag{23}$$

for a pressure tensor $P_{\alpha\beta}$ given by

$$P_{\alpha\beta} = \frac{\partial\mathcal{F}}{\partial(\partial_\alpha n)}(\partial_\beta n) - \mathcal{F}\delta_{\alpha\beta}, \tag{24}$$

where $\mathcal{F}=\psi-\mu_b n+\kappa(\partial_\gamma n)^2/2$ [34]. For our choice of ψ this gives

$$P_{\alpha\beta} = p(\mathbf{x})\delta_{\alpha\beta} + \kappa(\partial_\alpha n)(\partial_\beta n) \tag{25}$$

with

$$p(\mathbf{x}) = p_0 - \kappa n\nabla^2 n - \frac{\kappa}{2}(\partial_\gamma n)^2, \tag{26}$$

where $p_0 = n\partial_n\psi - \psi$ is the equation of state of the fluid.

III. BOUNDARY CONDITIONS

A. Partial wetting boundary conditions

In his paper on critical point wetting, Cahn showed how, by including short ranged surface-fluid interactions, the surface tensions σ_{sg} and σ_{sl} may be calculated [35] within a mean field framework. Cahn assumed that the fluid-solid interactions are short ranged such that they contribute a surface integral to the total free energy of the system. The total free energy becomes

$$\Psi = \int_V dV\left[\psi(T,n) + \frac{\kappa}{2}(\partial_\alpha n)^2\right] + \int_S dS\,\Phi(n_s). \tag{27}$$

Here, $\Phi(n_s)$ is a surface free energy density function which depends only on the density at the surface n_s and S is the surface bounding V.

Minimizing subject to natural boundary conditions (an explanation of natural boundary conditions may be found in, for example, Ref. [36]) (since n_s is unknown) gives an equilibrium boundary condition on the surface S. The boundary condition is

$$\kappa\hat{\mathbf{s}}\cdot\boldsymbol{\nabla} n = \frac{d\Phi}{dn_s}, \tag{28}$$

where $\hat{\mathbf{s}}$ is the unit normal to S pointing into the fluid. Following Cahn and de Gennes we choose to expand Φ as a power series [1,35]: a linear term only is sufficient for our purposes so we write $\Phi(n_s) = -\phi_1 n_s$ where ϕ_1 is a constant, which we call the wetting potential. Thus Eq. (28) becomes $\kappa\partial_\perp n = -\phi_1$.

The results for the surface tensions are

$$\sigma_{sg} = -\phi_1 n_c + \frac{\sigma}{2} - \frac{\sigma}{2}(1-\Omega)^{3/2}, \tag{29}$$

$$\sigma_{sl} = -\phi_1 n_c + \frac{\sigma}{2} - \frac{\sigma}{2}(1+\Omega)^{3/2}, \tag{30}$$

where $\Omega = \phi_1/\beta\tau\sqrt{2\kappa p_c}$ is the dimensionless wetting potential [22,35,37].

The wetting angle is found by substituting Eqs. (29) and (30) into Young's law [Eq. (1)]. The result is

$$\cos\theta_w = \frac{(1+\Omega)^{3/2}-(1-\Omega)^{3/2}}{2}. \tag{31}$$

Equation 31 is an equation for θ_w given a wetting potential Ω. A suitable inversion for the range $0<\theta_w<\pi$ is

$$\Omega = 2\,\mathrm{sgn}\left(\frac{\pi}{2}-\theta_w\right)\left[\cos\left(\frac{\alpha}{3}\right)\left\{1-\cos\left(\frac{\alpha}{3}\right)\right\}\right]^{1/2}, \tag{32}$$

where $\alpha = \arccos(\sin^2\theta_w)$ and $\mathrm{sgn}(x)$ gives the sign of x [37]. Therefore, by choosing a desired angle θ_w we can calculate the required wetting potential Ω.

The problem of incorporating wetting into a lattice Boltzmann scheme is in essence finding a way to include the boundary condition (28). Our algorithm can be thought of in three basic steps as follows. First we choose the desired wetting properties of a surface (i.e., the wetting angle θ_w). Next we calculate the required value of $\partial_\perp n$ using Eqs. (32) and (28). Lastly we use this value of $\partial_\perp n$ rather than a numerical

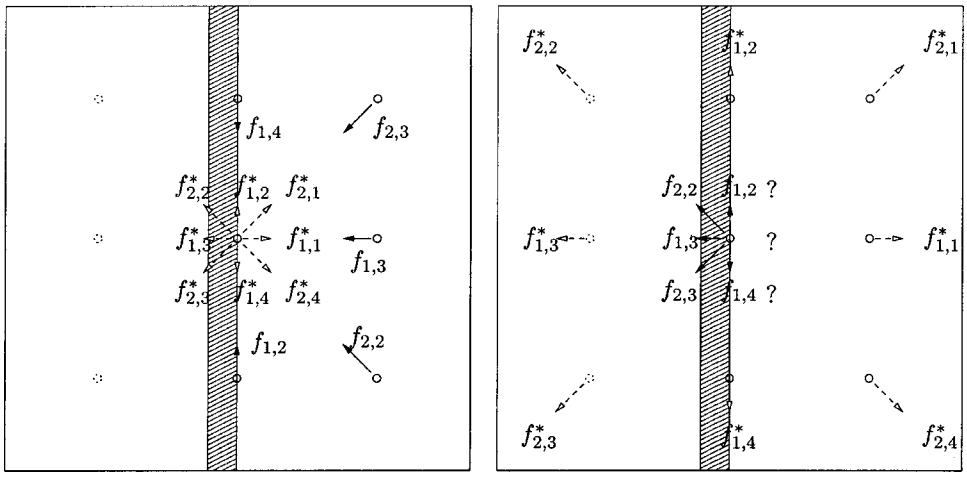

FIG. 1. The wall before and after streaming. Partial densities are shown by arrows: Dashed open headed arrows represent post collision values at time t, solid arrows precollision values at time $t+\Delta t$. The dashed lattice sites to the left of the wall are fictitious. After streaming $f^*_{1,3}$, $f^*_{2,2}$, and $f^*_{2,3}$ are outside the domain, while $f_{1,1}$, $f_{2,1}$, and $f_{2,4}$ are undetermined (denoted "?").

derivative when calculating f^{eq} at the wall. The details of the scheme can be found in Refs. [27] and [38], which show that the correct equilibrium angle is obtained within the range $30°<\theta_w<150°$ to within 2°.

B. Shear boundary conditions

In this paper we will be interested in sheared systems, where a velocity is required at the lattice edges. In order to close the lattice with walls rather than periodic boundary conditions we have developed a closure scheme which allow us to implement a no-slip condition *at the last lattice site* rather than between lattice sites. This is helpful because the wetting boundary conditions of Sec. III A are most easily imposed at a lattice site. The length of the system in the x direction, L_x, is $(N_x-1)\Delta x$.

Closing the lattice with flat walls leads to a problem of undetermined densities after the streaming step. For a wall along the line $x=0$ and fluid occupying $x>0$, Fig. 1 shows the problem at one lattice site: After streaming $f^*_{1,3}$, $f^*_{2,2}$, and $f^*_{2,3}$ have streamed out of the domain, while $f_{1,1}$, $f_{2,1}$, and $f_{2,4}$ are undetermined. To overcome this difficulty we choose the undetermined densities such that the fluid obeys a no-slip condition at the wall after the streaming step. Since we wish to impose shear, we take the wall velocity to be $u^{\text{wall}}\hat{\mathbf{y}}$. Recalling that $\Sigma_{\sigma i} f_{\sigma i} e_{\sigma i \alpha} = n u_\alpha$, the no-slip conditions give two equations for the three unknowns. The system is closed by making the choice $\overline{f}_{1,1}=f_{1,3}$. Solving the no-slip conditions for $\overline{f}_{2,1}$ and $\overline{f}_{2,4}$ then leaves us with

$$\overline{f}_{2,1}=\frac{1}{2}(\overline{n}u_y^{\text{wall}}+f_{1,4}+2f_{2,3}-f_{1,2}), \tag{33}$$

$$\overline{f}_{2,4}=\frac{1}{2}(-\overline{n}u_y^{\text{wall}}-f_{1,4}+2f_{2,2}+f_{1,2}), \tag{34}$$

where

$$\overline{n}=f_{0,0}+f_{1,2}+f_{1,4}+2(f_{1,3}+f_{2,2}+f_{2,3}). \tag{35}$$

One difficulty remains with this closure scheme: if the sum of $\overline{f}_{1,1}$, $\overline{f}_{2,1}$, and $\overline{f}_{2,4}$ at time $t+\Delta t$ is not equal to that of $f^*_{1,3}$, $f^*_{2,2}$, and $f^*_{2,3}$ at time t, then the streaming step does not conserve mass. To restore mass conservation on the system we note that $f_{0,0}$ is not present in the no-slip conditions. We can therefore adjust $f_{0,0}$ to conserve mass without affecting the imposed wall velocity. We therefore make a small adjustment to $f_{0,0}$:

$$\begin{aligned} f_{0,0}(\mathbf{x},t+\Delta t)=f^*_{0,0}(\mathbf{x},t)-\overline{f}_{1,1}(\mathbf{x},t+\Delta t)-\overline{f}_{2,1}(\mathbf{x},t+\Delta t) \\ -\overline{f}_{2,4}(\mathbf{x},t+\Delta t)+f^*_{1,3}(\mathbf{x},t)+f^*_{2,2}(\mathbf{x},t) \\ +f^*_{2,3}(\mathbf{x},t) \end{aligned} \tag{36}$$

which restores mass conservation to the system.

IV. SIMULATIONS OF A SHEARED LIQUID-GAS SYSTEM

The simulations we report here use a droplet held between two parallel plates of length L_y separated by a distance L_x. The system is closed by periodic boundaries in the y direction. The wetting conditions at the plates are chosen to be $\theta_w=90°$. We half fill the system with liquid ($n=n_l$) and half with gas ($n=n_g$). Equilibrium is a simple stripe pattern. Once equilibrium is achieved, the plates are moved with velocities $+V_0\hat{\mathbf{y}}$ and $-V_0\hat{\mathbf{y}}$ at $x=0$ and L_x. The system comes to a nonequilibrium steady state (as sketched in Fig. 2). The profiles of the two interfaces were recorded by measuring $\theta_1(x)$ and $\theta_2(x)$, the angles that the tangents to the two interfaces at x make with the wall at $x=0$ (see Fig. 2).

We varied L_x, keeping other parameters constant, to see how and if a dynamic contact angle could be defined. The results are shown in Fig. 3, with the parameter sets given in the caption. We see that the interfaces are effectively pinned to θ_w at the walls and are almost flat in the center of the system. As L_x increases the interface profiles appear to con-

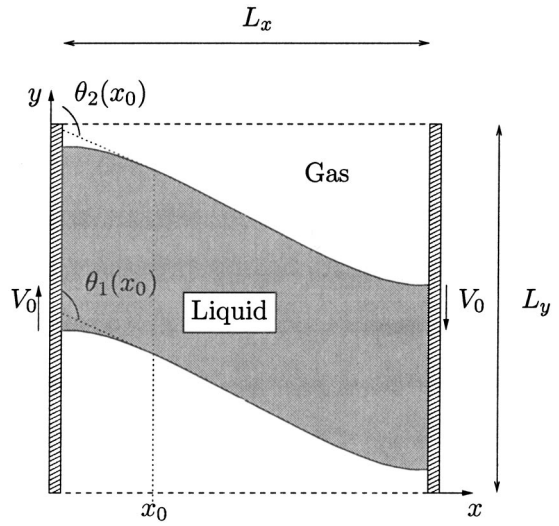

FIG. 2. The system in the steady state. The walls are sheared by applying velocities $+V_0\hat{\mathbf{y}}$ and $-V_0\hat{\mathbf{y}}$ at $x=0$ and L_x. Thus the interfaces are stationary. The system is characterized by $\theta_1(x)$ and $\theta_2(x)$, the angular profiles of the two interfaces. Neutral wetting conditions are applied at both walls, so that $\theta_1(0)=\theta_1(L_x)=\theta_2(0)=\theta_2(L_x)=\pi/2$.

verge toward a value, in the center of the system. To illustrate this, we plot $\theta_1^{\mathrm{Mid}}=\theta_1(x/L_x=0.5)$ against L_x in Fig. 4.

We now examine the system in Fig. 3(g) in more detail, as a precursor to an approximate analytic treatment for the average interface shape, $\overline{\theta}=(\theta_1+\theta_2)/2$. Observing that the curvature of the interface is highest at the walls, we plot the interfacial curvature $1/R$ against x for the system with $N_x=400$ in Fig. 5. (The curvature is defined as $1/R=d\theta_1/ds$ where s is the coordinate along the interface.) The curvature is approximately an odd function about $x/L_x=0.5$, dropping (rising) from a maximum (minimum) value at $x=0$ ($x=L_x$) and effectively flattening in the center.

It is enlightening to observe the way in which both the interface shape and fluid velocity are linked with this behavior of the curvature. We plot the velocity field in three regions of the system in Fig. 6. Figure 6(a) shows the interface and velocity field around the contact point at $x=0$, which is a region of high positive curvature. The column $i=1$ shows the no-slip condition where $(u_x,u_y)=(0,V_0)$. The interface is stationary (the system is in the steady state) but fluid is being continuously advected in the positive y direction. The mechanism whereby the interface is not advected with the fluid is found in the converging velocity field ($\boldsymbol{\nabla}\cdot\mathbf{u}<0$), which we interpret as condensation. The rate of advection of the interface with the fluid is balanced by condensation, which moves the interface in the opposite direction. This condensation is signaled by mass transfer across the interface from a region of low density (gas) to a region of high density (liquid).

Figure 6(b) shows the interface and velocity field around the center of the system, which is the region of essentially zero curvature. The velocity field is on the same scale as Fig. 6(a). Here there is no mass transfer across the interface and therefore no condensation/evaporation is required to maintain the steady state.

Figure 6(c) shows the interface and velocity field around the contact point at $x=L_x$, which is a region of high negative curvature [again on the same scale as Fig. 6(a)]. The column $i=400$ shows the no-slip condition at $x=L_x$ $[(u_x,u_y)=(0,-V_0)]$. Here we see mass transfer from liquid to gas which we interpret as evaporation (signaled by $\boldsymbol{\nabla}\cdot\mathbf{u}>0$). The stationary interface occurs due to the balance of advection with the flow and evaporation moving the interface in the opposite direction.

To illustrate the behavior of the velocity field more clearly, we plot both the parallel and perpendicular components of $\mathbf{u}$ at the interface, as a function of x/L_x, in Fig. 7. The perpendicular component $u_\perp$ behaves qualitatively in the same way as the curvature $1/R$. To illustrate how closely $u_\perp$ and $1/R$ are related we plot $R^{-1}/\max(R^{-1})$ and $u_\perp/\max(u_\perp)$ against x/L_x in Fig. 8. From this figure we postulate that the curvature of the interface is proportional to the perpendicular component of velocity through it. We write

$$\frac{1}{R}=cu_\perp \tag{37}$$

introducing c as the constant of proportionality.

We have performed extensive simulations to determine how c depends on system parameters. By measuring the exponents of each parameter separately we conclude that $c\propto\eta_c\Delta n^2/\xi\sigma n_c^2$ where $\eta_c=\nu_{\mathrm{visc}}n_c$, $\Delta n=n_l-n_g$. Figure 9 shows the observed value of c against $\eta_c\Delta n^2/\xi\sigma n_c^2$, and shows that constant of proportionality is approximately 0.75. With c determined Eq. (37) can be written as

$$\frac{1}{R}=\alpha\frac{\eta_c u_\perp}{\sigma\xi}\left(\frac{\Delta n}{n_c}\right)^2, \tag{38}$$

with $\alpha=0.75$. In the following section we present a scaling argument to justify Eq. (38).

V. A SCALING ARGUMENT FOR *c*

To motivate the functional form for c we begin by considering the steady state continuity equation evaluated at the center of the interface ($n=n_c$):

$$n_c[\boldsymbol{\nabla}\cdot\mathbf{u}]_{n=n_c}=-[\mathbf{u}\cdot\boldsymbol{\nabla}n]_{n=n_c}. \tag{39}$$

On the right-hand side of Eq. (39) the dot product picks out the component of $\mathbf{u}$ perpendicular to the interface, $u_\perp$, and we approximate $\boldsymbol{\nabla}n$ as the change in density across the interface divided by the interface width, i.e., $\Delta n/\xi$. Equation (39) then becomes

$$n_c[\boldsymbol{\nabla}\cdot\mathbf{u}]_{n=n_c}\approx-u_\perp\frac{\Delta n}{\xi}. \tag{40}$$

We next want to find an approximation for $[\boldsymbol{\nabla}\cdot\mathbf{u}]_{n=n_c}$. In Fig. 10 we plot $\partial_x u_x$ and $\partial_y u_y$ for a typical system. From it,

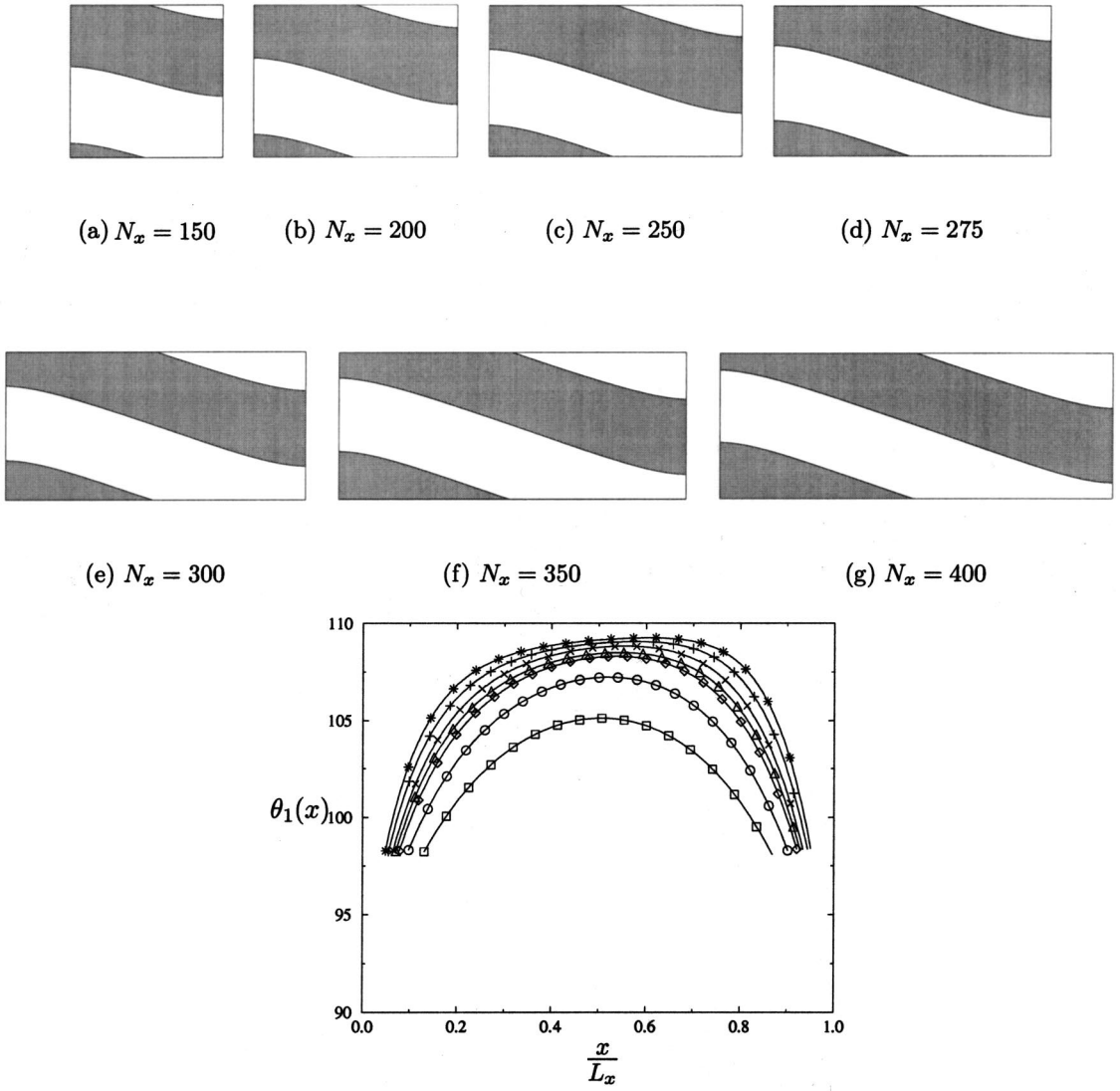

FIG. 3. Top, real space configurations for simulations with increasing N_x. The parameters used were $N_y=150$, $\tau_f=0.8$, $V_0=2.5\times10^{-4}$, $\kappa=0.0025$, $n_c=3.5$, $p_c=0.125$, and $\beta\tau=0.03$. Bottom, corresponding interface profiles $\theta_1(x)$ against x/L_x. The symbols are $N_x=150$, □; $N_x=200$, ○; $N_x=250$, ◇; $N_x=275$, △; $N_x=300$, ×; $N_x=350$, +; $N_x=400$, *.

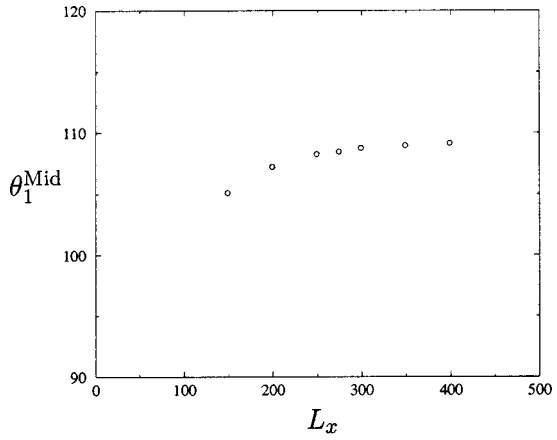

FIG. 4. The midpoint angle $\theta_1^{\mathrm{Mid}}=\theta_1(x/L_x=0.5)$ against L_x for the seven systems in Fig. 3.

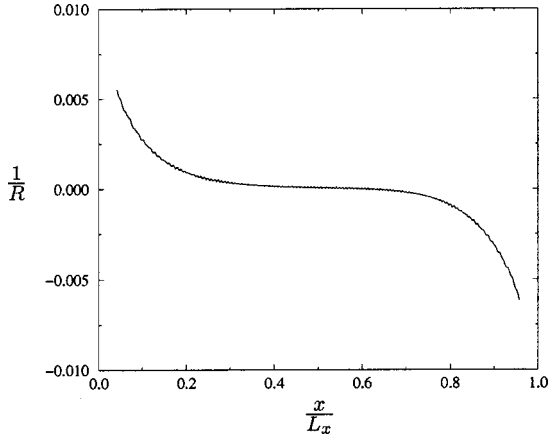

FIG. 5. The curvature of the interface $1/R$ against x/L_x for the system in Fig. 3(g).

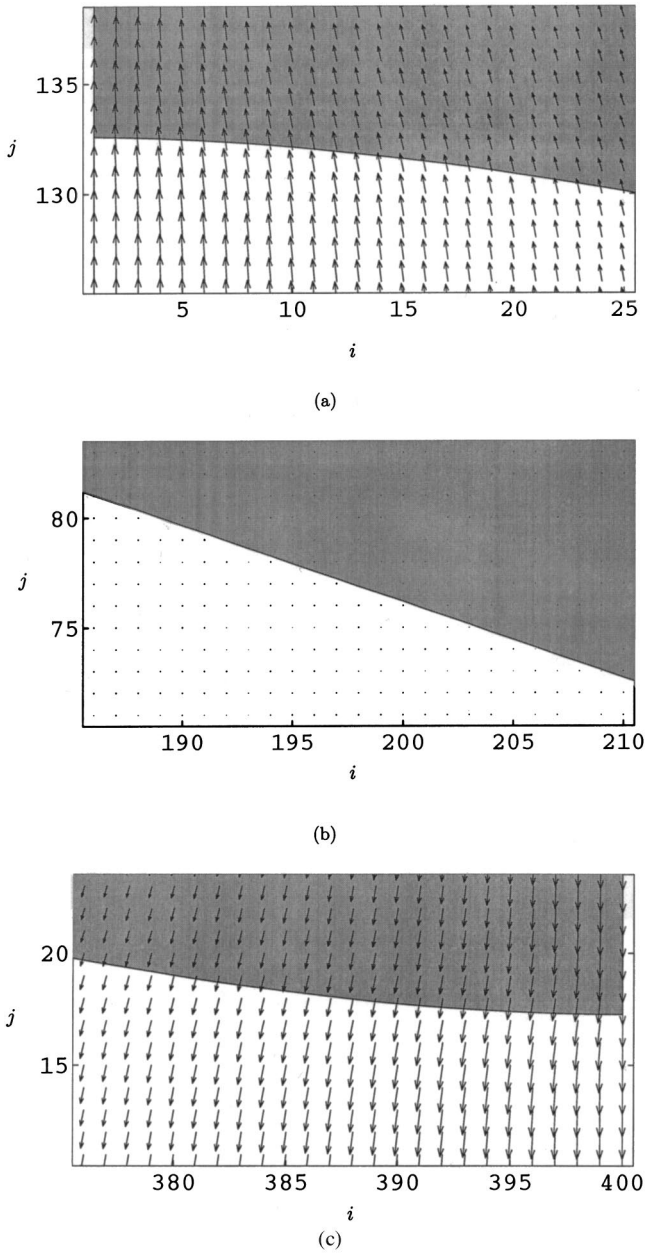

FIG. 6. The interface and fluid velocity field in three regions of one interface for the largest sheared system in Fig. 3. We remind the reader that dark (light) shading represents liquid (gas) and that the lattice coordinates are i and j.

we conclude that, apart from exactly at the walls, an approximation for $\partial_y u_y$ will serve as an approximation for $\boldsymbol{\nabla}\cdot\mathbf{u}$ in the interface.

In order to find the value of $\partial_y u_y$ in the interface, we write the y component of the Stokes equation out in full:

$$\partial_x P_{yx}+\partial_y P_{yy}=\nu_{\mathrm{visc}}\partial_x[n(\partial_y u_x+\partial_x u_y)] + \nu_{\mathrm{visc}}\partial_y[n(\partial_x u_x+3\partial_y u_y)]. \quad (41)$$

By integrating Eq. (41) across a gently curved interface and examining the dominant terms, we will show that

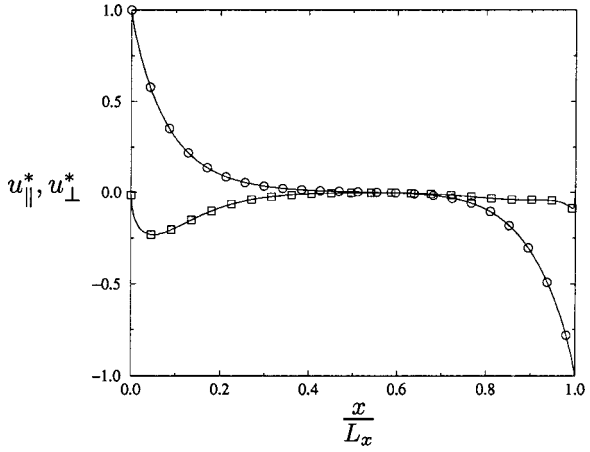

FIG. 7. The parallel (□) and perpendicular (○) velocities (normalized by V_0) in the interface plotted against x/L_x.

$$\frac{\sigma}{R}\approx-\nu_{\mathrm{visc}}\Delta n\,\partial_y u_y, \quad (42)$$

which will serve as an approximation for $\partial_y u_y$.

Integrating the left-hand side of Eq. (41) gives (see Appendix B for details)

$$\int dy[\partial_x P_{yx}+\partial_y P_{yy}]=\frac{\sigma}{R}+\Delta p_0, \quad (43)$$

where $\Delta p_0=p_l-p_g$, the pressure difference across the interface.

We now want to find the dominant viscous terms when the right-hand side of Eq. (41) is integrated with respect to y, from the gas phase to the liquid phase. Numerical examination of the seven viscous terms arising in Eq. (41) shows that three terms give the dominant contributions to the integral. These are

$$v_1=\int dy\,3\nu_{\mathrm{visc}}(\partial_y n)(\partial_y u_y), \quad (44)$$

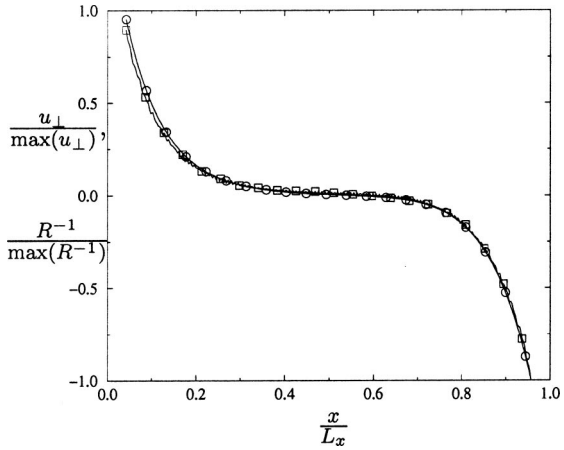

FIG. 8. The curvature (○) and perpendicular velocity (□) at the interface, both normalized by their maximum value.

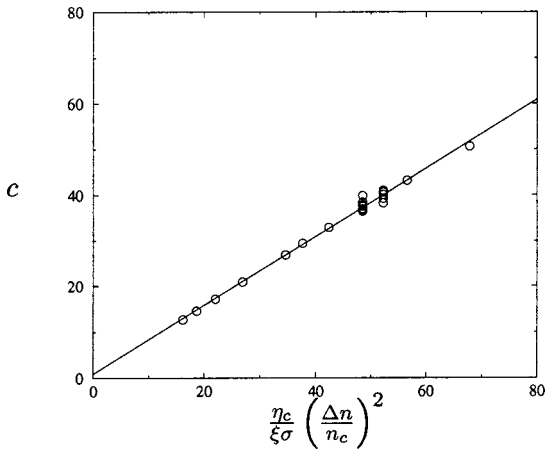

FIG. 9. The measured values of c against $\eta_c \Delta n^2/\xi\sigma n_c^2$. The straight line is the fit to the data, giving $\alpha = 0.75$.

$$v_2 = \int dy\, \nu_{\mathrm{visc}} n(\partial_{xx} u_y), \tag{45}$$

and

$$v_3 = \int dy\, 3\nu_{\mathrm{visc}} n(\partial_{yy} u_y). \tag{46}$$

Figure 11 shows v_1, v_2, and v_3 as a function of x/L_x and also σ/R against x/L_x, the dominant term from the pressure tensor integration. From Fig. 11 we see that none of these viscous terms dominates over the others. However, to a good approximation $v_1 = -v_2 = -v_3$. Choosing to work with v_1 for later convenience, we set the sum of the three main viscous terms equal to the largest term from Eq. (43), which gives

$$-v_1 = -\int dy\, 3\nu_{\mathrm{visc}} (\partial_y n)(\partial_y u_y) = \frac{\sigma}{R}. \tag{47}$$

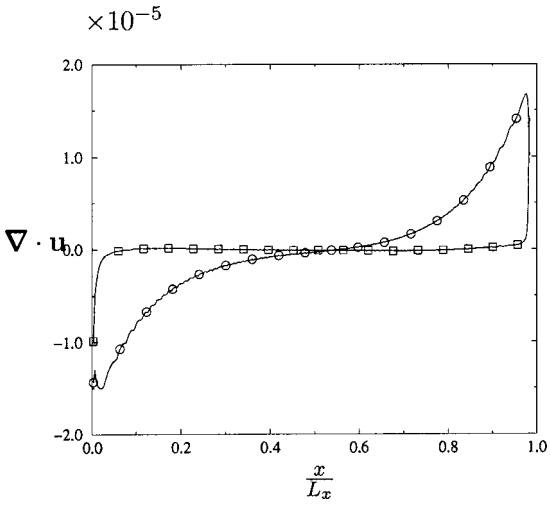

FIG. 10. Terms of $\nabla \cdot \mathbf{u}$ at the interface against x/L_x. The symbols are $\partial_x u_x$ □ and $\partial_y u_y$ ○.

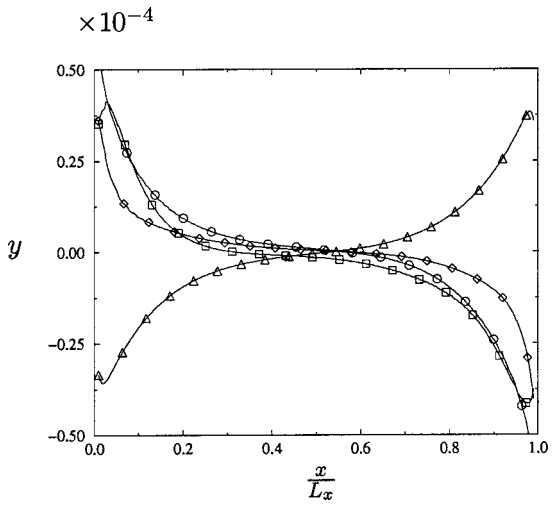

FIG. 11. The integrated viscous terms from the Stokes equation. The symbols are $y = v_1$, △; $y = v_2$, ◇; $y = v_3$, □. For comparison, the dominant pressure term σ/R is also shown ($y = \sigma/R$, ○).

To show that Eq. (47) holds, we plot $-v_1$ and σ/R in Fig. 12. To complete the argument, we now find an approximation for $\partial_y u_y$ by estimating the integral v_1. The integrand is sharply peaked at the interface due to the factor of $\partial_y n$, over which distance we may consider $\partial_y u_y$ to remain constant at $[\partial_y u_y]_{n=n_c}$. By approximating $\partial_y n$ to $\Delta n/\xi$ and taking ξ to be proportional to the width of the integration, we write

$$\xi 3\nu_{\mathrm{visc}} \frac{\Delta n}{\xi} [\partial_y u_y]_{n=n_c} \propto -\frac{\sigma}{R}. \tag{48}$$

We now substitute Eq. (48) into Eq. (40) and rearrange to get

$$\frac{\sigma}{R} = \alpha \frac{\eta_c u_\perp}{\xi} \left(\frac{\Delta n}{n_c}\right)^2, \tag{49}$$

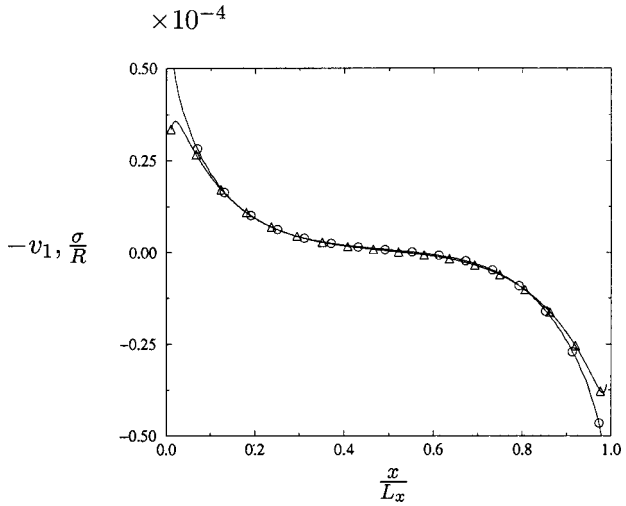

FIG. 12. The terms of Eq. (47) against x/L_x (○ and △ denote σ/R and $-v_1$, respectively). We conclude that Eq. (47) is a good approximation, with the errors increasing very close to the walls.

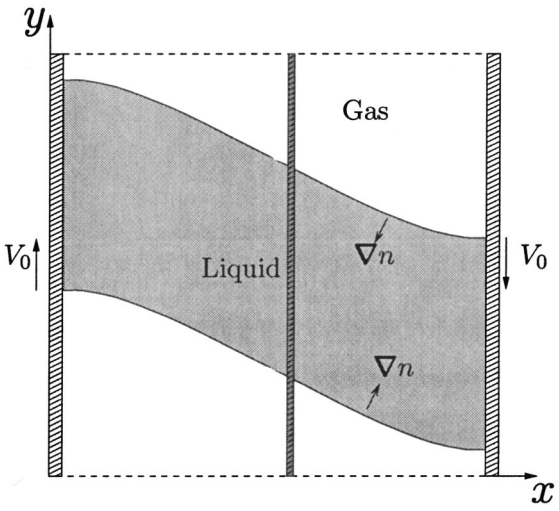

FIG. 13. We consider the total force per unit area along the y direction acting on thin fluid elements such as the one shown. As a visual reminder the direction of ∇n is indicated on the two interfaces.

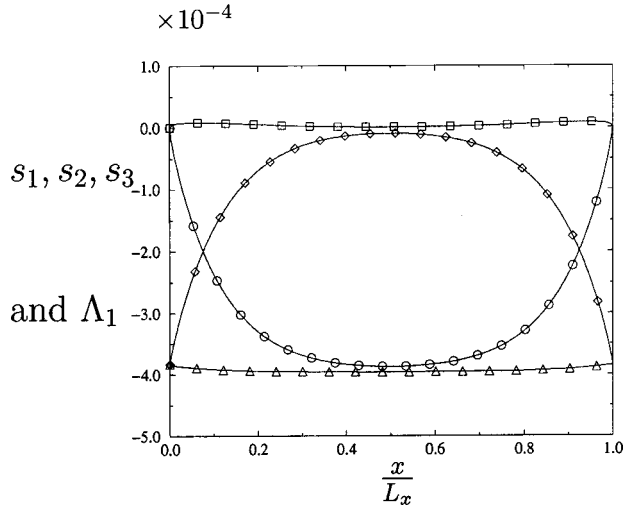

FIG. 14. The total stress terms arising from Eq. (51). The symbols are: ○, $s_1=-\Sigma\Delta x P_{yx}$; ◇, $s_2=\Sigma\Delta x\,\eta\partial_x u_y$; □, $s_3=\Sigma\Delta x\,\eta\partial_y u_x$. △ denotes the sum of these three terms [i.e., Λ_1 in Eq. (51)].

where $\eta_c=n_c\nu_{\rm visc}$ and α is a numerical factor. In words, Eq. (49) says that the perpendicular component of fluid velocity through a curved interface is proportional to its curvature R^{-1}. Equation (49) is none other than Eq. (38) rearranged and completes our motivation for Eq. (38).

VI. STRESS FORMULA

In this section we present an approximate analytic treatment of the system described in Sec. IV, based on considering the stresses in the system.

The system is in a steady state which implies that the total force per unit area along y direction acting on a thin fluid element whose normal is in the x direction, i.e., the total yx stress, $\int dy\,\sigma_{yx}$, is constant across the system (see Fig. 13). The yx component of the stress tensor is

$$\sigma_{yx}=-P_{yx}+\eta(\partial_y u_x+\partial_x u_y). \tag{50}$$

Multiplying σ_{yx} by Δx and summing over the y direction (i.e., the coordinate j) gives

$$-\sum_{j=1}^{N_y}\Delta x P_{yx}+\sum_{j=1}^{N_y}\Delta x(\eta\partial_x u_y+\eta\partial_y u_x)=\Lambda_1, \tag{51}$$

where Λ_1 is a constant. Figure 14 shows the terms of Eq. (51) for a typical system. We see that $\Sigma\Delta x\,\eta\partial_y u_x\approx 0$ and so this term in Eq. (51) is neglected.

To proceed, we now relate the two remaining terms of Eq. (51) to the angular positions of the interfaces. Combining this with Eq. (38) will lead to a differential equation for $\overline{\theta}$ which we will solve.

From Appendix B we use Eq. (B5) to write the pressure tensor term as

$$-\sum_{j=1}^{N_y}\Delta x P_{yx}=\sigma(\cos\theta_1+\cos\theta_2). \tag{52}$$

We next make an approximation that u_y is a function of x alone, so that the viscous stress term in Eq. (51) becomes

$$\sum_{j=1}^{N_y}\Delta x\,\eta\partial_x u_y=\overline{\eta}L_y\frac{d}{dx}u_y, \tag{53}$$

where $\overline{\eta}=(\Sigma_{j=1}^{n_y}\Delta x\,\eta)/L_y$. For the systems with equal amounts of gas and liquid $\overline{\eta}=\eta_c=\nu_{\rm visc}n_c$.

Using Eqs. (52) and (53), Eq. (51) for the balance of stress becomes

$$2\sigma\cos\overline{\theta}\cos\Delta\theta+L_y\overline{\eta}\frac{d}{dx}u_y=\Lambda_1, \tag{54}$$

where we have used a double angle formula for $(\cos\theta_1+\cos\theta_2)$. In doing so, we have defined $\overline{\theta}=(\theta_1+\theta_2)/2$ and $\Delta\theta=(\theta_1-\theta_2)/2$. The asymmetry between the interfaces is small so that $\Delta\theta\approx 0$ and $\cos\Delta\theta\approx 1$.

We now relate u_y to the curvature of the interfaces using Eq. (38). Recalling (from Appendix B) that $R^{-1}=d(-\cos\theta_I)/dx$ we can write

$$u_\perp^{(I)}=-\frac{\xi}{\alpha\eta_c}\left(\frac{n_c}{\Delta n}\right)^2\frac{d}{dx}(\sigma\cos\theta_I), \tag{55}$$

where the superscript I ($=1$ or 2) refers to the interface with angle θ_I. We approximate u_y by the average perpendicular fluid velocity through both interfaces

$$u_y=\frac{u_\perp^{(1)}+u_\perp^{(2)}}{2}=-\frac{\xi\sigma}{\alpha\eta_c}\left(\frac{n_c}{\Delta n}\right)^2\frac{d}{dx}(\cos\overline{\theta}\cos\Delta\theta). \tag{56}$$

Substituting Eq. (56) into Eq. (54) gives a second order differential equation for $\cos\overline{\theta}$:

$$\frac{d^2}{dx^2}\cos\overline{\theta}-\frac{2\alpha}{L_y\xi}\left(\frac{\Delta n}{n_c}\right)^2\cos\overline{\theta}=\Lambda_2, \tag{57}$$

where Λ_2 is a constant absorbing Λ_1 and system parameters.

The solution to Eq. (57) is

$$\cos\overline{\theta}=-\frac{\Lambda_2}{k^2}+A(e^{-kx}+e^{-k(L_x-x)}), \tag{58}$$

where $k=\sqrt{2\alpha/L_y\xi}(\Delta n/n_c)$ and A is an integration constant to be determined from the boundary conditions. [Only one integration constant is present in Eq. (58) since we have built the solution to respect the $x\to L_x-x$ symmetry of the system.]

Recalling that at $x=0$, $u_y=V_0$, Eq. (56) gives us the constant A:

$$V_0=-\frac{\xi\sigma}{\alpha\eta_c}\left(\frac{n_c}{\Delta n}\right)^2(-k)A[e^{-kx}-e^{-k(L_x-x)}]_{x=0}. \tag{59}$$

Rearranging Eq. (59) gives

$$A=\frac{\eta_c V_0}{\sigma}\frac{\Delta n}{n_c}\sqrt{\frac{\alpha L_y}{2\xi}}[1-e^{-kL_x}]^{-1}. \tag{60}$$

We can deduce the constant Λ_2 by using the fact that $\overline{\theta}=\pi/2$ at $x=0$. This procedure gives

$$\Lambda_2=\sqrt{\frac{2\alpha^3}{L_y\xi^3}}\left(\frac{\Delta n}{n_c}\right)^3\frac{\eta_c V_0}{\sigma}\frac{1+e^{-kL_x}}{1-e^{-kL_x}}. \tag{61}$$

Putting Eqs. (60) and (61) into Eq. (58) gives the solution for $\overline{\theta}$ as

$$\overline{\theta}=\arccos\left[\frac{\eta_c V_0}{\sigma}\frac{\Delta n}{n_c}\sqrt{\frac{\alpha L_y}{2\xi}}\left(\frac{e^{-kx}+e^{-k(L_x-x)}}{1-e^{-kL_x}}-\frac{1+e^{-kL_x}}{1-e^{-kL_x}}\right)\right]. \tag{62}$$

Equation (62) is an equation for the average angle $(\theta_1+\theta_2)/2$. The only fit parameter, α, has been determined over a large range of data to be 0.75. The comparison between a simulation profile and Eq. (62) has no remaining free parameters.

We choose the system with $N_x=300$ from the simulation in Fig. 3(e). In Fig. 15 we plot $\overline{\theta}$ from this simulation and Eq. (62), with $\alpha=0.75$, against x/L_x. The fit is good with the largest deviation being less than 1°. Some error is not surprising given the approximations inherent in the derivation.

To compare the formula for $\overline{\theta}$ further, in Fig. 16 we plot numerical data for $\overline{\theta}^{\mathrm{Mid}}[=\overline{\theta}(x/L_x=0.5)]$ against L_x^{-1}. The results approach a constant value as $L_x\to\infty$ which we may identify as a dynamic contact angle. This corresponds to the angular position of the interface in the region where there is no evaporation or condensation, i.e., where the curvature is zero. Results from the analytic approximation Eq. (62) are also plotted in Fig. 16. Equation (62) predicts a dynamic contact angle

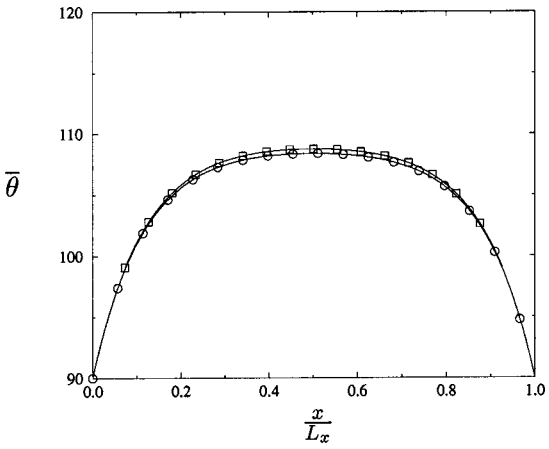

FIG. 15. Observed $\overline{\theta}$ (□) and theoretical $\overline{\theta}$ (○) against x/L_x, for the system in Fig. 3(e). The maximum difference between the result from Eq. (62) and the data is less than 1°.

$$\overline{\theta}_\infty=\arccos\left[-\frac{\eta_c V_0}{\sigma}\frac{\Delta n}{n_c}\sqrt{\frac{\alpha L_y}{2\xi}}\right] \tag{63}$$

which, for the parameters in Fig. 3 gives $\overline{\theta}_\infty=108°$ [40].

The treatment presented here does not offer any insight into the behavior of $\Delta\theta$ (i.e., the difference between θ_1 and θ_2). The asymmetry in the interface profiles can reasonably be expected on the basis of the velocity fields observed near the contact line (Fig. 6). This limitation means that the analytic approximation is applicable only to the case of neutral wetting.

VII. DISCUSSION

In this paper we have described a lattice Boltzmann scheme for the simulation of contact line motion in liquid-

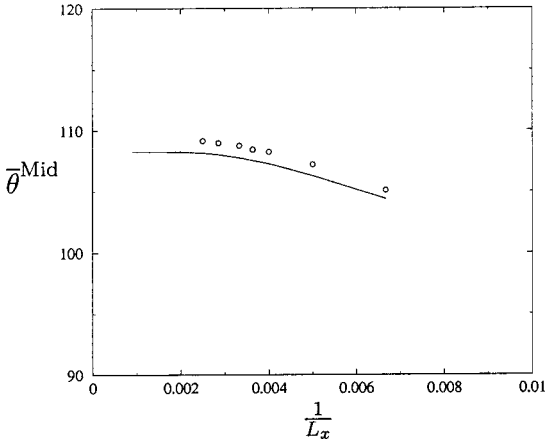

FIG. 16. Values of $\overline{\theta}^{\mathrm{Mid}}[=\overline{\theta}(x/L_x=0.5)]$ (○) against $1/L_x$, for the systems in Fig. 3. The line is the result of Eq. (62), which takes the value 108° at $L_x^{-1}=0$. The maximum difference between Eq. (62) and the data is less than 1°.

gas systems. Careful implementation of the thermodynamic boundary condition allowed us to fix the static contact angle in the simulations. We then considered the behavior of a sheared interface. Under no-slip boundary conditions on the fluid velocity the interface moves via evaporation/condensation. The fluid velocity perpendicular to the interface is proportional to its curvature. Near the contact line the high curvature allows evaporation/condensation while in the center of the system the curvature is essentially zero and no mass transfer takes place. We exploited this proportionality and the constancy of the stress in the steady state to derive an analytic approximation for the angular position of the interface.

The moving contact line of the diffuse interface liquid-gas model in a different geometry has been previously studied analytically by Seppecher [22]. The author matched an external flow (appropriate to a wedge of one fluid displacing a second) to an inner solution, where the diffuse interface model was used. Seppecher showed that the curvature of the interface in the inner region drives a mass flux across the interface. The author also measured an apparent contact angle as the angle defined by the interface when the curvature was effectively zero.

The system studied in this paper has similarities to and differences from that studied by Seppecher. The most noticeable difference is that, in the geometry employed here, no wedge flow exists far from the contact lines. The velocity fields and interface shapes are therefore qualitatively different between the studies. The principal similarity is the way in which the curvature and mass flux allow the interface to relax and remain stationary under no-slip conditions on the fluid velocity.

Recently, interest in sheared interfaces has grown. Travasso *et al.* [39] solved a similar geometry to that described here for the Ising model with a non-conserved order parameter (i.e. model A) and found a delocalization transition for the interface above a critical shear rate. Jacqmin [23] and Chen *et al.* [24] have published work for model H (binary fluids), which we consider in the companion paper. Chen *et al.* also considered model B. To the authors' knowledge, this is the first study of a liquid-gas system under the shear boundary conditions of Fig. 2.

We have shown how a diffused interface model can overcome the contact line problem, even under strict no-slip conditions on the fluid velocity. However, a central question of contact line motion remains: what is the physical mechanism which generates the slip of the contact line? Mesocale modeling techniques, and the lattice Boltzmann method in particular, allow a wide choice of boundary conditions for the density and velocity fields. They do not, however, offer information on the validity of those boundary conditions. This must be obtained from microscopic simulation and experiment. Molecular dynamics simulations, which have started to investigate this question, show that slip of the fluid velocity can occur in certain circumstances around the contact line [16–20]. Experimental work may also help resolve the question if techniques can be used to probe the interface on small length scales. Indeed using lattice Boltzmann simulations to investigate the relative effects of slip and evaporation/condensation on the droplet motion and then comparing to experiment may be a way to assess the importance of each mechanism in a given physical system.

ACKNOWLEDGMENTS

We thank P. Papatzacos and C. Pooley for helpful discussions. A.B. acknowledges EPSRC and Unilever plc. for financial support.

APPENDIX A: COEFFICIENTS FOR THE LIQUID-GAS MODEL

The coefficients are

$$A_2=\frac{p_0}{8c^2}+\frac{\nu_{\mathrm{visc}}}{4c^2}(u_x\partial_x n+u_y\partial_y n), \tag{A1}$$

$$A_1=2A_2, \quad A_0=n-12A_2, \tag{A2}$$

$$B_2=\frac{n}{12c^2}, \quad B_1=4B_2, \tag{A3}$$

$$C_2=-\frac{n}{16c^2}, \quad C_1=2C_2, \quad C_0=12C_2, \tag{A4}$$

$$D_2=\frac{n}{8c^4}, \quad D_1=4D_2, \tag{A5}$$

$$G_{2xx}=\frac{\kappa}{16c^4}[(\partial_x n)^2-(\partial_y n)^2]+\frac{\nu_{\mathrm{visc}}}{8c^4}(u_x\partial_x n-u_y\partial_y n), \tag{A6}$$

$$G_{2xy}=G_{2yx}=\frac{\kappa}{8c^4}[(\partial_x n)(\partial_y n)]+\frac{\nu_{\mathrm{visc}}}{8c^4}(u_x\partial_y n+u_y\partial_x n), \tag{A7}$$

$$G_{2yy}=-G_{2xx}, \tag{A8}$$

$$G_{1\alpha\beta}=4G_{2\alpha\beta} \quad \text{for all } \alpha,\beta. \tag{A9}$$

APPENDIX B: CURVATURE, SURFACE TENSION, AND LAPLACE'S LAW

We derive some useful results concerning the surface tension and curvature of the interface.

The surface tension of the liquid-gas interface is given by

$$\sigma=\kappa\int dg(\partial_g n)^2. \tag{B1}$$

Here, g is the coordinate perpendicular to the interface and the limits of the integration are across an interface.

In Sec. VI we needed to calculate the surface tension when the interface lies at an angle θ_I to the y direction and the integration is over y (see Fig. 17). In this case Eq. (B1) becomes

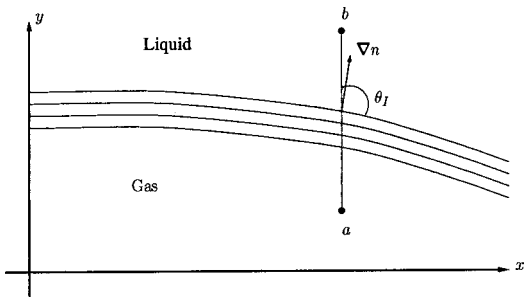

FIG. 17. Contours of the interface between gas and liquid. The line ab show the path of integration. The direction of ∇n is constant along ab provided that $R \gg \xi$. The angle of the interface θ_I is measured from the y axis.

$$\sigma = \kappa \int dy (\nabla n)^2 \sin\theta_I . \tag{B2}$$

To make the connection with the pressure tensor we note that ∇n makes an angle $\theta_I - \pi/2$ with the y direction (see Fig. 17). Therefore we may write

$$\sin\theta_I = \frac{\partial_y n}{|\nabla n|} \tag{B3}$$

and

$$\cos\theta_I = -\frac{\partial_x n}{|\nabla n|} . \tag{B4}$$

Multiplying Eq. (B2) by $-\cos\theta_I$ and using Eqs. (B3) and (B4) gives

$$-\sigma\cos\theta_I = \kappa \int dy (\partial_y n)(\partial_x n) = \int dy\, P_{yx} . \tag{B5}$$

Thus the relation between surface tension and the off-diagonal term of the pressure tensor is clear.

We now show that differentiating Eq. (B5) leads to σ/R, where R is the radius of curvature of the interface. Recalling that the definition of curvature of a line is the rate of change of angle with coordinate along the line, we have

$$\frac{1}{R} = \frac{d\theta_I}{ds} , \tag{B6}$$

where s is the coordinate along the interface. In terms of dx $(= ds \sin\theta_I)$ this may be rewritten as

$$\frac{1}{R} = \frac{d\theta_I}{dx}\sin\theta_I = \frac{d}{dx}(-\cos\theta_I) . \tag{B7}$$

Differentiating Eq. (B5) now leads to

$$\frac{\sigma}{R} = \frac{d}{dx}\int dy\, P_{yx} . \tag{B8}$$

Equation (B8) makes the link between curvature and the pressure tensor.

To derive Laplace's law, we recall that in equilibrium the divergence of the pressure tensor vanishes

$$\partial_x P_{yx} + \partial_y P_{yy} = 0. \tag{B9}$$

Since P_{yx} is zero on the limits of integration in Eq. (B8) the order of integration and differentiation can be interchanged. Equation (B8) becomes

$$\frac{\sigma}{R} = \int dy\, \partial_x P_{yx} = -\int dy\, \partial_y P_{yy} = p_{\text{gas}} - p_{\text{liquid}} . \tag{B10}$$

Equation (B10) is Laplace's law.

[1] P.G. de Gennes, Rev. Mod. Phys. **57**, 827 (1985).
[2] T. Young, Philos. Trans. R. Soc. London **95**, 65 (1805).
[3] C. Huh and L.E. Scriven, J. Colloid Interface Sci. **35**, 85 (1971).
[4] E.B. Dussan V. and S.H. Davis, J. Fluid Mech. **65**, 71 (1974).
[5] E.B. Dussan V., J. Annu. Rev. Fluid Mech. **11**, 371 (1979).
[6] L.M. Hocking, J. Fluid Mech. **79**, 209 (1977).
[7] C. Huh and S.G. Mason, J. Colloid Interface Sci. **60**, 11 (1977).
[8] L.M. Hocking and A.D. Rivers, J. Fluid Mech. **121**, 425 (1982).
[9] R.G. Cox, J. Fluid Mech. **168**, 169 (1986).
[10] C.G. Ngan and E.B. Dussan V., J. Fluid Mech. **209**, 191 (1989).
[11] E.B. Dussan V., Ramé, and S. Garoff, J. Fluid Mech. **230**, 97 (1991).
[12] J.A. Marsh, S. Garoff, and E.B. Dussan V., Phys. Rev. Lett. **70**, 2778 (1993).
[13] Q. Chen, E. Ramé, and S. Garoff, Phys. Fluids **7**, 2631 (1995).
[14] Q. Chen, E. Ramé, and S. Garoff, J. Fluid Mech. **337**, 49 (1997).
[15] E. Ramé and S. Garoff, J. Colloid Interface Sci. **177**, 234 (1996).
[16] P.A. Thompson and M.O. Robbins, Phys. Rev. Lett. **63**, 766 (1989).
[17] J. Koplik, J.R. Banavar, and J.F. Willemsen, Phys. Fluids A **1**, 781 (1989).
[18] P.A. Thompson, W.B. Brinckerhoff, and M.O. Robbins, J. Adhes. Sci. Technol. **7**, 535 (1993).
[19] P.A. Thompson and M.O. Robbins, Phys. Rev. A **41**, 6830 (1990).
[20] C. Denniston and M.O. Robbins, Phys. Rev. Lett. **87**, 178302 (2001).
[21] J.-L. Barrat and L. Bocquet, Faraday Discuss. **112**, 119 (1999).
[22] P. Seppecher, Int. J. Eng. Sci. **34**, 977 (1996).
[23] D. Jacqmin, J. Fluid Mech. **402**, 57 (2000).
[24] H.-Y. Chen, D. Jasnow, and J. Viñals, Phys. Rev. Lett. **85**, 1686 (2000).
[25] D. Grubert and J.M. Yeomans, Comput. Phys. Commun. **121**, 236 (1999).
[26] J.-C. Desplat, I. Pagonabarraga, and P. Bladon, Comput. Phys. Commun. **134**, 273 (2001).

[27] A.J. Briant, P. Papatzacos, and J.M. Yeomans, Philos. Trans. R. Soc. London, Ser. A **360**, 485 (2002).
[28] M.R. Swift, W.R. Osborn, and J.M. Yeomans, Phys. Rev. Lett. **75**, 830 (1995).
[29] P. Bhatnagar, E.P. Gross, and M.K. Krook, Phys. Rev. **94**, 511 (1954).
[30] Y.H. Qian, D. d'Humières, and P. Lallemand, Europhys. Lett. **17**, 479 (1992).
[31] M.R. Swift, E. Orlandini, W.R. Osborn, and J.M. Yeomans, Phys. Rev. E **54**, 5041 (1996).
[32] D.J. Holdych, D. Rovas, J.G. Georgiadis, and R.O. Buckius, Int. J. Mod. Phys. C **9**, 1393 (1998).
[33] S. Hou, Q. Zou, S. Chen, G. Doolen, and A.C. Cogley, J. Comput. Phys. **118**, 329 (1995).
[34] D.M. Anderson, G.B. McFadden, and A.A. Wheeler, Annu. Rev. Fluid Mech. **30**, 139 (1998).
[35] J.W. Cahn, J. Chem. Phys. **66**, 3667 (1977).
[36] H. Sagan, *Introduction to Calculus of Variations* (McGraw-Hill, New York, 1969).
[37] P. Papatzacos, Transp. Porous Media **49**, 139 (2002).
[38] A.J. Briant, D. Phil., University of Oxford (2003).
[39] R.D.M. Travasso, A.J. Bray, and A. Cavagna, J. Phys. A **34**, 195 (2001).
[40] In Ref. [27] we presented data to show that the midpoint angle converged to an apparent contact angle and estimated this angle by a plot against $1/L_x$. Here we present a theory which suggests a better way to perform this extrapolation. We also note that the data presented here is slightly different from that in Ref. [27] due to inconsistencies in the initial conditions and system sizes in that work.